Co-funded by the European Union

Research Fund for Coal & Steel

Hybrid energy storage system using post-mining infrastructure (HESS)

Deliverable 3.2.

Technical parameters of the example underground water reservoir model

31.12.2024

PROJECT	
Project number	**101112380**
Project name	**Hybrid energy storage system using post-mining infrastructure**
Project acronym:	**HESS**
Call	**RFCS-2022**
Topic	**RFCS-01-2022-RPJ**
Type of action	**RFCS-PJG**
Service	**REA/B/01**

DOCUMENT PROPERTIES

Document Number	**D.3.2.**
Document Title	**Technical parameters of the example underground water reservoir model**
Document responsible	**SUT**
Target dissemination level	**PU**
Document authors	**Grzegorz Smolnik (SUT)** **Konrad Kołodziej (SUT)** **Adam Niewiadomski (SUT)** **Marcin Lutyński (SUT)**
Data of the document	**31.12.2024**

Table of contents

1. Introduction

In order to store water pumped from the surface in the underground reservoir that is converted from a former mine working it is necessary to select and identify workings suitable for the construction of the reservoir. In this study it is assumed that the lower part of the shaft is flooded along with the surrounding workings. In general, the purpose of any support is to protect against destructive stresses from the rock mass (rock pressure) by various types of lining. In the case of shafts, it is most commonly thick-walled reinforced concrete or cast-iron segmental tubing. For underground galleries these are most commonly steel arch supports or other types of supports in the vicinity of shafts, e.g. brick support. All these measures aim to ensure stability in the working. Water under hydrostatic pressure that is discharged to the lower reservoir under cycling operation will exert force on the lining in the opposite direction to the rock mass pressure. As a result, the water pressure should not add to the rock mass stresses but instead counteract it, thereby reducing excavation convergence. It is anticipated that additional lining will not be required along most of the shaft part yet additional support is required in the galleries as it was explained in Deliverable 2.2 It is also anticipated that supplementary sealing using a flexible coating is necessary.

Unlike the lining of the majority of other mining excavations, the shaft lining is designed and constructed to be relatively airtight due to the presence of pressurized aquifers within the rock mass, which is another advantage of using as much of the shaft space as possible. Furthermore, the temperature of the rock mass increases with depth, at an average rate of approximately 3°C per 100 meters in most Polish mines. At a depth of 1000 meters, the temperature exceeds 35°C and remains stable, thereby limiting heat transfer from the storage facility. Therefore, it is crucial to take the temperature factor into account when designing conversion of underground workings into energy storage.

2. Goal of the work

In this deliverable a complex model for the assessment of shaft failure based on the Coulomb criterion and temperature was developed and the example calculation in UDEC software based on the selected underground working have been presented. Additionally, based on the developed model a PRESS-SHAFT application has been created that is able to calculate failure of the shaft casing under excess pressure and/or temperature.

3. Analysis of the stability of a circular cross-section mining excavation

During the excavation and operation of shafts—whether utilized as mining excavations, conduits for high-pressure water transport in hydroelectric power plants, or energy storage facilities such as compressed air systems—the primary issue concerning their stability remains similar.
Two main risks of stability loss are observed: fracturing caused by exceeding the ultimate tensile strength and cracking resulting from high shear stresses.

To prevent these highly unfavorable phenomena, stress state analysis around the shaft is typically performed, assuming the rock mass as a linearly elastic, isotropic medium, and using the Coulomb (Coulomb-Mohr) failure criterion.
Although attempts to apply elastic-plastic models for the stability analysis of boreholes and shafts have been undertaken since the 1940s, over time, it became evident that the fewer parameters involved in equations derived from elasticity theory provide a significant advantage. As a result, the classical approach continues to be the most widely used.
The Coulomb failure criterion describes the relationship between shear stress and normal stress at the strength limit and is typically expressed as:

$$\tau = c + \sigma_n \tan\varphi \qquad (1)$$

where τ- shear strength, c- cohesion, σn – normal stress, ϕ- angle of internal friction (Fig. 1).

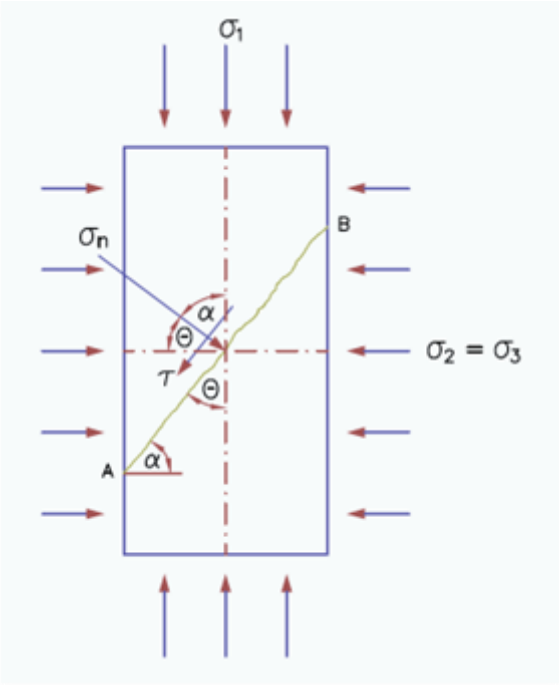

Fig. 1. Stress distribution on the plane (surface) of failure in a certain volume of material subjected to triaxial compression.

However, this criterion can also be expressed in terms of principal stresses, in which case it takes the following form:

$$\sigma_1 = 2\,c\,\frac{1+\sin\varphi}{1-\sin\varphi} + \sigma_3\frac{1+\sin\varphi}{1-\sin\varphi} \qquad (2)$$

where σ_1 is the maximum principal stress at the failure limit, and σ_3 is the minimum principal stress (Figure 2).

The form of the Coulomb criterion expressed in terms of principal stresses is equivalent to the linear, fundamental failure criterion for rocks

$$\sigma_1 = R_c + B\,\sigma_3 \qquad (3)$$

where: R_c- uniaxial compressive strength, and B is the coefficient determining the rate of increase of the maximum principal stress at the failure limit as the minimum principal stress increases.

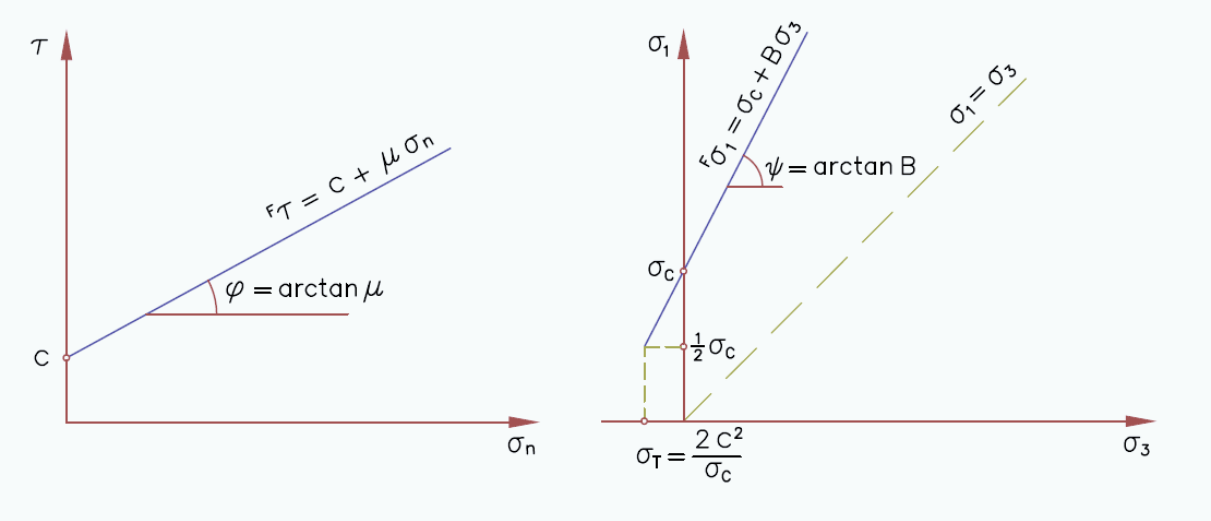

Fig. 2. The Coulomb failure criterion expressed in terms of stresses acting in the failure plane and in terms of principal stresses.

As can be observed, the following relationships exist between cohesion, the internal friction angle, the uniaxial compressive strength, and the constant B (see e.g. Jaeger et al., 2007; Kwaśniewski, 2000):

$$c = \frac{R_C}{2\sqrt{B}} \quad \text{and} \quad B = \frac{1+\sin\varphi}{1-\sin\varphi} = tan^2\left(45° + \frac{\varphi}{2}\right) \qquad (4)$$

The construction of a vertical excavation with a circular cross-section will disturb the original state of stress occurring in the rock massif, which will cause a redistribution of stresses in its vicinity, with extreme stress values occurring on the contour of the excavation.

Equations describing the stress state around a circular cross-section excavation indicate that the stress state depends solely on the values of the initial stresses in which the excavation is created. Neither the elastic constants nor even the radius or diameter of the excavation appear in these equations. Therefore, considerations regarding the stress state on the excavation boundary hold true for rocks with significantly varying deformability as well as for shafts with very different diameters. Moreover, they are equally valid for boreholes with a diameter of only a few centimetres and for shafts/workings with a diameter exceeding 10 meters.

This fact has led to some confusion in the past. Some underground excavation designers concluded that since the stress state on the excavation boundary does not depend on its size, the stability of the excavation would also be unaffected by its size. If the rock mass were an ideal isotropic medium, free from fractures and discontinuities, and perfectly linearly elastic, such a conclusion would be justified. However, this is not valid when considering real rock masses.

Even if the stresses remain the same, in an actual rock mass—heterogeneous, inelastic, layered-block, and fractured—the stability of the excavation depends on the size of the excavation relative to the size of the rock blocks within the mass. Consequently, increasing the dimensions

of the excavation in a typical rock mass, although it does not increase the stress values on its boundary, certainly increases the risk of stability loss. Failure to consider this fact has previously led to serious problems with roof collapses and the loss of excavation stability (Hoek and Brown, 1980).

The need to take into account the heterogeneous, layer-block structure of the rock mass when analysing the possibility of using shafts or roadways with a circular cross-section as compressed air energy storage or elements of pumped-storage power plant infrastructure will be discussed in this study in its further part. The problem is all the more serious because it is the shafts with diameters of at least several meters that are in fact boreholes with an extremely large diameter.

The impact of fluids under high pressure (e.g. water in hydroelectric power plant systems, crude oil in boreholes, drilling mud in drilling in natural gas extraction or compressed air in energy storage) significantly affects the state of stress both in the contour of the excavation and in its surroundings, but does not change the fact that extreme stress values will occur on the outline of the excavation.

There, too, the destruction, if it occurs, will be initiated. Therefore, the analysis of shaft/working stability must include checking whether the values of stresses created on the walls of the opening (shaft) are acceptable (safe) or whether they lead to failure in accordance with the adopted strength condition.

The creation of a mining excavation disrupts the pre-existing equilibrium state in the rock mass and causes a redistribution of the initial stresses. When analysing the stress distribution around the shaft/working, a plane stress state is typically considered, where a flat disk (simulating a section of the rock mass) is loaded at its edges by the components of the initial rock pressure in the horizontal directions σ_x and σ_y.

Expressing the components of the stress state in polar coordinates, and taking into account the boundary conditions shown in Figure 3, the solution for the stress state is obtained in the following form (Kirsch, 1898):

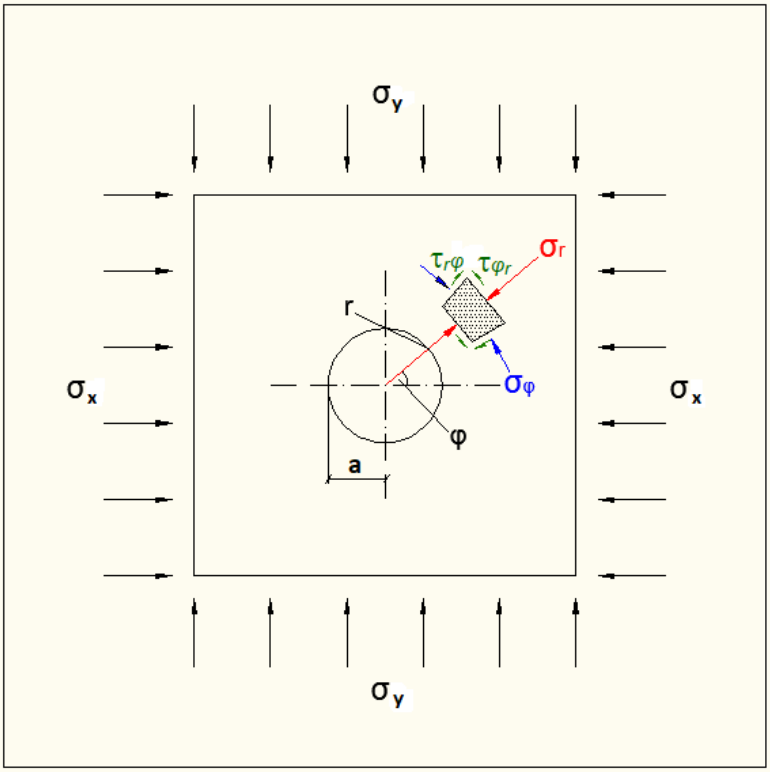

Fig. 3. Stress state around a circular cross-section excavation.

Radial stresses σ_r:

$$\sigma_r = \frac{\sigma_y}{2}\left[1 - \frac{a^2}{r^2} - \left(1 - 4\frac{a^2}{r^2} + 3\frac{a^4}{r^4}\right)cos2\varphi\right] + \\ + \frac{\sigma_x}{2}\left[1 - \frac{a^2}{r^2} + \left(1 - 4\frac{a^2}{r^2} + 3\frac{a^4}{r^4}\right)cos2\varphi\right] \quad (5)$$

circumferential stresses σ_φ:

$$\sigma_\varphi = \frac{\sigma_y}{2}\left[1 + \frac{a^2}{r^2} + \left(1 + 3\frac{a^4}{r^4}\right)cos2\varphi\right] + + \frac{\sigma_x}{2}\left[1 + \frac{a^2}{r^2} - \left(1 + 3\frac{a^4}{r^4}\right)cos2\varphi\right] \quad (6)$$

tangential stress $\tau_{r\varphi} = \tau_{\varphi r}$

$$\tau_{r\varphi} = \tau_{\varphi r} = \frac{\sigma_y - \sigma_x}{2}\left(1 + 2\frac{a^2}{r^2} - 3\frac{a^4}{r^4}\right)sin2\varphi \quad (7)$$

where:

σ_y – horizontal component of the initial stress in the direction *y [MPa]*,

σ_x – component of the horizontal primary stress in the direction of *x [MPa]*,

a – excavation radius [m],

r, φ – Polar coordinates [m], [°].

On the boundary of the excavation contour (where $r = a$) the stress state reduces to the following form:

$$\sigma_r = 0 \quad (8)$$
$$\sigma_\varphi = \sigma_y(1 + 2cos2\varphi) + \sigma_x(1 - 2cos2\varphi)$$
$$\tau_{r\varphi} = \tau_{\varphi r} = 0$$

The value of the circumferential stress also depends on the location of the point on the excavation boundary. In particular, the following points can be distinguished:

along the direction x (φ = 0°, φ = 180°): (9)
$$\sigma_\varphi = 3\sigma_y - \sigma_x$$
along the direction y (φ = 90°, φ = 270°):
$$\sigma_\varphi = 3\sigma_x - \sigma_y$$
in intermediate points (φ = 45°, φ = 135°,φ = 225° i φ = 315°):
$$\sigma_\varphi = \sigma_y + \sigma_x$$

The most favourable case from a geomechanical point of view occurs when the horizontal stresses acting on the lining/support of a circular cross-section shaft/working have equal values. First, there is no risk of tensile stresses occurring on the excavation boundary; second, the stress state is uniform throughout its lining; and third, the concentration of compressive stresses is no greater than the sum of the initial stresses.

3.1 Stability of a vertical shaft subjected to the pressure of water and isotropic horizontal stresses

For a vertical shaft subjected to horizontal stresses of equal value (px = py) and exposed to pressure, such as compressed air or water, acting on its inner lining surface, the stresses on the excavation boundary are equal:

$\sigma_r = p_w$
$\sigma_\theta = 2\ p_x - p_w$ (10)
$\sigma_z = p_z$

Depending on the value of the main stresses and their mutual relation to each other, several conditions can be determined when the shaft casing may be destroyed (cracked).

Let us first consider the case when $\sigma_\theta > \sigma_z > \sigma_r$ on the excavation boundary. According to the Coulomb failure criterion, failure will occur when:

$\sigma_\theta = R_c + B\ \sigma_r$ (11)

By introducing equations (10) into equation (11) we get:

$$p_w = \frac{2p_x - R_c}{B+1} \quad (12)$$

If the compressed air or water pressure falls below the value determined in Equation (12), the shaft casing will fail due to exceeding the shear strength.

Next, suppose that the pressure of the medium in the shaft builds up so that:
$\sigma_r > \sigma_z > \sigma_\theta$. Coulomb's condition will then take the following form:

$\sigma_r = R_c + B\ \sigma_\theta$ (13)

After introducing equations (10) into equation (13), we obtain the second condition of shaft stability:

$$p_w = \frac{2Bp_x + R_c}{B+1} \quad (14)$$

If the water or compressed air pressure rises above the value determined in Equation (14), the shaft casing will fail due to exceeding the shear strength. Therefore, having obtained both the minimum and the maximum pressure value of the working medium in the shaft, we can determine the range of pressure values for which shear failure does not occur and the stability of the shaft is maintained.

In cases where significant differences exist between the values of horizontal and vertical stresses, the Coulomb failure criterion may still be satisfied (and failure of the lining may occur) whether σ_z is the maximum or the minimum principal stress. Considering this observation will limit the safe pressure range for compressed air or water in the shaft, but it is necessary for the proper design of the energy storage system.

A comprehensive analysis of the safe pressure range for water or compressed air in the shaft requires considering all six possible permutations of the three principal stresses σ_θ, σ_z i σ_r. Two of them for $\sigma_\theta > \sigma_z > \sigma_r$ and $\sigma_r > \sigma_z > \sigma_\theta$ analysed above, let us start the analysis of the other four with the case where the $\sigma_z > \sigma_\theta > \sigma_r$. Coulomb's condition then has the following form:

$$\sigma_z = R_c + B\,\sigma_r \quad (15)$$

After introducing equations (10) into equation (15), we get the relation:

$$p_w = \frac{p_z - R_c}{B} \quad (16)$$

Destruction of the casing/working will occur in this case when the pressure of water falls below the value determined in equation (16).

The last condition defining the minimum safe value of water or air pressure in the shaft is the relationship when σ_z is the least principal stress, i.e. the situation when: $\sigma_\theta > \sigma_r > \sigma_z$.

Coulomb's condition then takes the form:

$$\sigma_\theta = R_c + B\,\sigma_z \quad (17)$$

Introducing equations (10) into equation (17) we get:

$$p_w = 2p_x - R_c - Bp_z \quad (18)$$

A decrease in the pressure of the medium in the shaft below the value given by equation (18) means the occurrence of damage to the casing as a result of exceeding the permissible value of shear stresses inside it.

There are two conditions to consider defining the maximum safe value of air or water pressure in the shaft in addition to the one already taken into account (14). Let us first consider the case when p_w (= σ_r becomes intermediate principal stress: $\sigma_z > \sigma_r > \sigma_\theta$.

The form of the Coulomb condition is then as follows:

$\sigma_z = R_c + B\,\sigma_\theta$ (19)

After introducing equations (10) into equation (19), we obtain the following condition for the stability of the shaft:

$$p_w = \frac{2Bp_x + R_c - p_z}{B} \quad (20)$$

If the compressed air or water pressure rises above the value determined in Equation (20), the shaft casing will fail due to exceeding the shear strength.

The last condition defining the possibility of damage or destruction of the tight (impermeable) shaft lining due to exceeding the shear strength, and at the same time the third condition limiting the maximum value of water or compressed air pressure in the shaft derives from the following configuration of principal stresses: $\sigma_r > \sigma_\theta > \sigma_z$.

According to Coulomb's condition, destruction occurs when:

$\sigma_r = R_c + B\,\sigma_z$ (21)

After introducing equations (10) into equation (21), we get the relation:

$$p_w = R_c + B\,p_z \quad (22)$$

All these relationships are presented collectively in Table 1.

In the stability analysis of a shaft as a compressed air energy storage or an element of pumped-storage power plant infrastructure, it should be remembered that with an increase in the value of air or water pressure inside the shaft, the circumferential stress $\sigma\theta$ may take on negative values (see Equations 10).

Table 1. Conditions leading to shear failure of a shaft with an impermeable casing.

Variant	$\sigma_1 \geq \sigma_2 \geq \sigma_3$	Destruction (damage) to the shaft lining occurs when:
1	$\sigma_\theta \geq \sigma_z \geq \sigma_r$	$p_w \leq \frac{2p_x - R_c}{B+1}$
2	$\sigma_r \geq \sigma_z \geq \sigma_\theta$	$p_w \geq \frac{2Bp_x + R_c}{B+1}$
3	$\sigma_z \geq \sigma_\theta \geq \sigma_r$	$p_w \leq \frac{p_z - R_c}{B}$
4	$\sigma_\theta \geq \sigma_r \geq \sigma_z$	$p_w \leq 2p_x - R_c - Bp_z$
5	$\sigma_z \geq \sigma_r \geq \sigma_\theta$	$p_w \geq \frac{2Bp_x + R_c - p_z}{B}$
6	$\sigma_r \geq \sigma_\theta \geq \sigma_z$	$p_w \geq R_c + B\,p_z$

This may lead to a phenomenon analogous to hydraulic fracturing, known in petroleum engineering or geoengineering more broadly and used, for example, to measure stress values in the rock mass. Tension failure will occur if:

$\sigma_\theta < -R_r$ (23)

Incorporating equations (10) into equation (23) we obtain:

$$p_w = 2p_x + R_r \qquad (24)$$

If the water pressure in the shaft reaches the value given by equation (24), a crack will form in the lining.

Therefore, the equation (24) serves, in addition to the six previously analyzed conditions, as an additional constraint on the permissible pressure of the medium in the shaft. The range of safe compressed air or water pressures, considering shaft stability, can be presented graphically (Figure 4).

The graph was created based on the elegant method proposed by Guenot (1987) to present the effect of drilling fluid pressure on the stability of the borehole depending on the stress state in the rock mass (see also Maury, 1993).

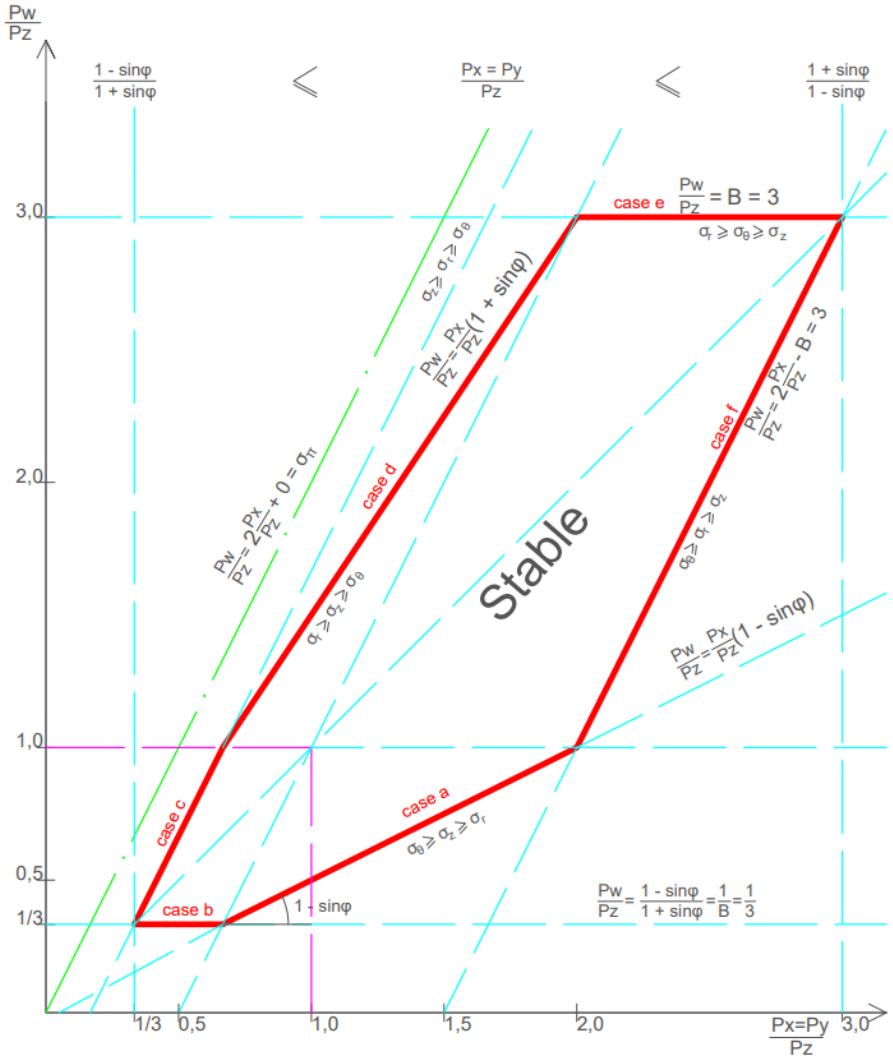

Fig. 4. Graphical representation of the stability conditions of the shaft lining subjected to the pressure of compressed air or water.

On the x-axis, the values of horizontal (isotropic) pressure are shown, referenced to the vertical pressure in the rock mass. The y-axis represents the ratio of compressed air or water pressure in the shaft to the vertical pressure in the rock mass. The graph was created based on Coulomb failure criterion, assuming that the material has zero cohesion and a friction angle of 30°. The area inside the polygon defines the pressure range that ensures the stability of the shaft as an energy storage facility for compressed air or water. Stress states outside the polygon area indicate damage (failure) of the lining/support. Each side of the polygon corresponds to one of the six conditions defining shear failure, with an indication of which specific condition it relates to. The figure also shows a line representing the value of the medium pressure in the shaft, above which failure due to tension will occur. If the air or water pressure in the shaft exceeds the threshold value indicated by this line, a vertical crack will form in the shaft lining. For the conditions shown in Figure 4, this type of failure is always preceded by shear failure. Despite the elegance of this method of presentation, as shown in Table 1, it is not easily used to read the safe pressure range in the compressed air or water energy storage system in the shaft.

For this purpose, it is easier to use the modified diagram shown in Figure 5. On the x-axis, the values of lithostatic pressure are marked ($p_x=p_y=p_z$) and the axis of elevations directly represents the pressure value of the working medium in the shaft.

Assuming the same internal friction angle (30°) – typical for many rocks and concretes – and a tensile limit strength of 4 MPa on the concrete support and a uniaxial compressive limit strength of 24 MPa, it is easy to identify both the dangerous pressures and depths in the shaft where problems may occur.

An increase in the compressed air or water pressure inside the shaft creates the risk of lining cracking, which poses a danger for low values of horizontal stresses acting in the rock mass, i.e., at shallow depths near the surface. It can be seen that the assumed maximum value of the compressed air or water pressure in the energy storage system, equal to 8 MPa, could generate a crack (fracture) for horizontal stresses lower than 2 MPa, which corresponds to a lithostatic stress state at depths from the surface to about 80 m.

If the concrete used has a tensile strength of about 6 MPa, lining cracking under the maximum pressure of water or compressed air in the shaft can only occur at very shallow depths, near the surface, close to the shaft bottom (up to about 40 m, with the same other parameters). The need to install the upper cover of the compressed air storage system, as a reinforced concrete plug of approximately 20 m thickness, ensures that even this tensile strength of the concrete significantly limits issues with shaft lining cracking, even at the closest parts near the surface.

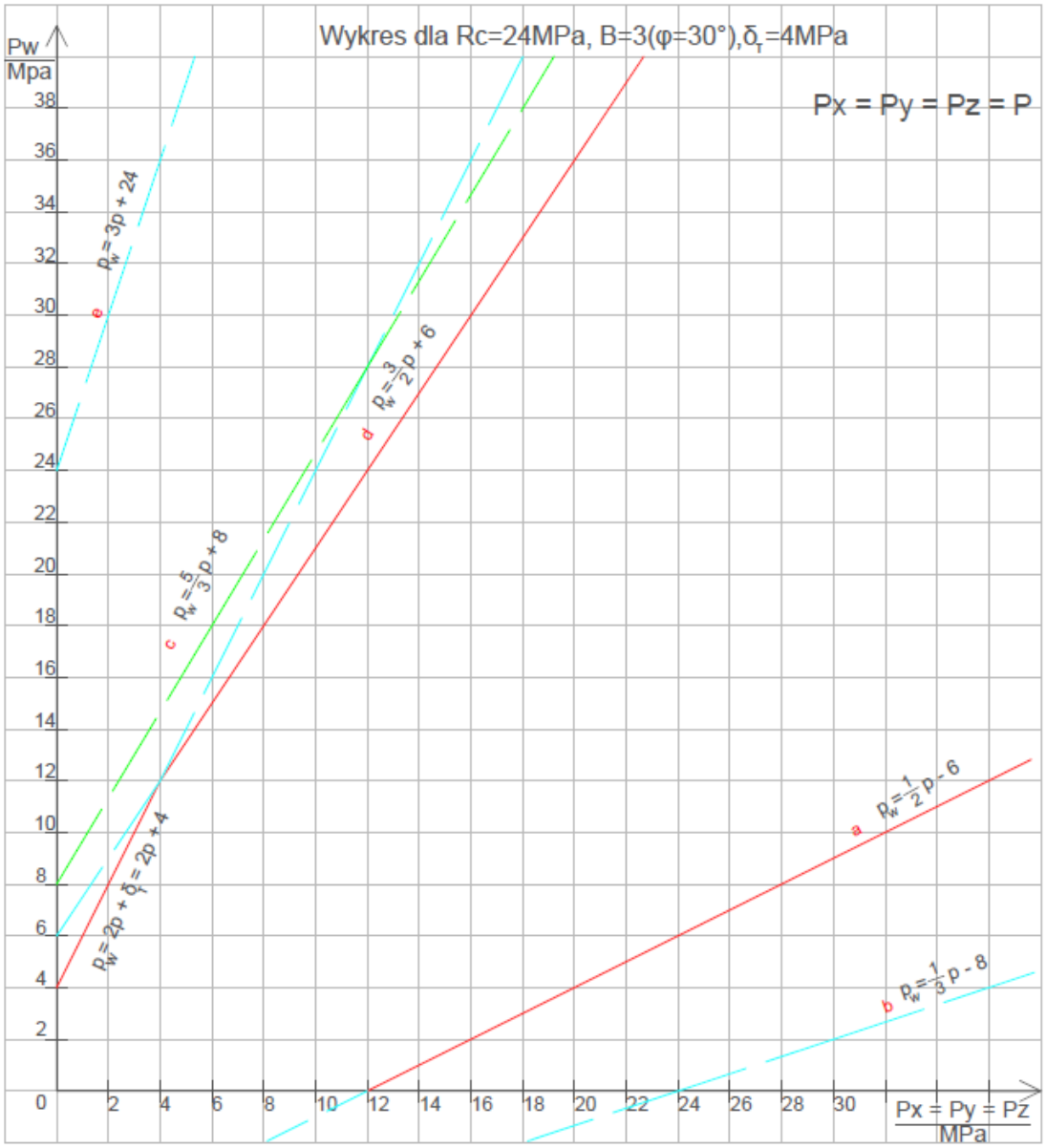

Fig. 5. Graphical representation of the stability conditions of the shaft lining with higher compressive strength.

Low air or water pressure in the shaft can be a problem of shear damage. The largest extent of the potential damage zone applies to situations before the shaft was adapted for energy storage. With the influence of only air or water pressure equal to the atmospheric pressure, cracking can occur from a depth of about 500 m (p_x=p_y=p_z=12 MPa). A higher compressive strength of concrete and an increase in its internal friction angle shift this boundary to greater depths. For example, increasing the concrete compressive strength from 24 MPa to 35 MPa causes the shear failure risk to begin at a depth nearly 50% deeper, i.e., around 730 m. Using concrete with a compressive strength (Rc) of 45 MPa would extend the safe zone to a considerable depth of 930 m.

Of course, the shaft lining during mining operation should withstand these loads without failure. However, due to factors such as the aging of the concrete lining or reduced maintenance towards the end of the shaft's mining life, the depth ranges indicated by the above analysis highlight areas where more detailed inspections should be conducted due to potential damage.

Compressed air in the shaft or water at greater depths has a stabilizing effect on the shaft casing, and so in the selected case, even the minimum expected air pressure value in the storage of 2 MPa moves the upper limit of the potential damage zone by about 150 m down the shaft ($p_x=p_y=p_z$=16 MPa). Air or water with a pressure of 8 MPa would allow the range of the safe zone to increase to a depth of about 1150 m ($p_x=p_y=p_z$=28 MPa).

The above analyses assume that the shaft lining and the rock layers in the immediate vicinity of the shaft are drained, and consequently, that only negligibly small pore pressures occur. If, however, significant pore pressures are present, it is necessary to consider this in the stability analysis. The role of pore pressure in geomechanics is well known and leads to the use of effective stresses as proposed by Terzaghi (1943). If the pore pressure is denoted as pf, the effective stress □' is the difference between the total (normal) stress σ and the pore pressure:

$$\sigma' = \sigma - p_f \qquad (25)$$

Equation (25) is widely used in soil and rock mechanics, but in a strict sense, it seems to describe the effect of pore pressure on the stress state only in materials with low strength, poorly or unconsolidated. Maurice A. Biot (1941, 1962) showed that the effective stress in rocks is given by a slightly modified equation:

$$\sigma' = \sigma - \alpha p_f \qquad (26)$$

Where the coefficient α ισ in the range:

$$n_p < \alpha \leq 1 \qquad (27)$$

The lower limit is porosity n_p (Total), that is, the ratio of the volume of pores in a rock to its total volume.

Taking into account the pore pressure in the analysis of the stability of the shaft as an energy storage of compressed air or water can be carried out in the same way as above, noting that the Coulomb condition expressed in the effective stress convention will take the form:

$$\sigma_1 - \alpha p_f = 2\,c\,\frac{1+\sin\varphi}{1-\sin\varphi} + \left(\sigma_3 - \alpha p_f\right)\frac{1+\sin\varphi}{1-\sin\varphi} \qquad (28)$$

and introducing it in the analysis of subsequent variants as shown earlier.

3.2 Stored medium temperature impact

Another important aspect to consider is the influence of the temperature of the medium (compressed air or water) in the shaft on the stability of the structure. Although the predicted temperatures of 30-40 °C will not cause any significant changes in the values of strength and strain parameters of rocks and concrete, they will be a source of thermal stresses. What will be

their value, and will they deteriorate the operating conditions of the enclosure and increase the risk of damage to it, or will their impact be positive and reduce the likelihood of fracturing and shear cracking?

The presence of a well-insulated, but occasionally under high temperature tank inside the shaft will be a source of heat maintaining a non-seasonally constant change in quasi-constant temperature in the forecast range of 30-40 °C. This will cause heating of the shallower parts of the shaft/workings and also - perhaps, depending on the depth of the shaft - slight cooling of the deepest parts of the casing.

The temperature of the shaft lining at the stage of its mining use is influenced by the temperature of the rocks at a given depth and the temperature of the air flowing inside it. The former is not subject to seasonal fluctuations and depends on the geothermal degree of the rock mass (temperature gradient). Assuming its average value for the Upper Silesian Coal Basin of the order of 0.03 °C/m, we can see that at a depth of one kilometre the temperature of the rocks increases by about 30 °C. Thus, for deep shafts, reaching below 1000 m, the primary temperatures of the rocks can be in the range of 40-50 °C. Of course, the shallower, closer to the surface, the lower the temperature and in a significant part of the shaft depth range it will be in the order of a dozen or twenty degrees Celsius.

The temperature of the air flowing through the shaft depends both on the outside temperature of the atmospheric air and is subject to strong seasonal changes, but also on the purpose of the shaft and the related direction of air flow. Ventilation shafts transport the so-called used air from the mine pit to the outlet on the surface. The temperature of this air, even in the deepest mines, is not high, despite the high primary temperature of the rocks at these depths - limited by mining regulations, it is reduced by air conditioning systems. In a typical mine, its range may correspond to that expected for a compressed air energy storage (30-40 °C).

In intake shafts, which most of them serve as, the flow of atmospheric air from the surface into the mine determines its temperature. Changes over the course of a day, but especially over the course of a year, can be significant. High flow velocity causes that even in winter, the air at the lower levels of the shaft does not have time to warm up, and generally, its temperatures in such shafts are lower both in summer and especially in winter compared to the projected temperatures in the shaft as an energy storage system.

Long-term heating of the casing and rocks in its immediate vicinity will cause an increase in stress. The ring and vertical stresses on the contour of the roadway will increase by the value of the given relation (Fjaer et. al., 1992, zob. też Habib i Berest, 1993):

$$\Delta\sigma = \frac{E}{1-\nu}\alpha_T\left(T - T_f\right) \qquad (29)$$

where ν - Poisson's ratio, E- Young's modulus, αT – coefficient of thermal expansion, Tf- initial temperature of rock or concrete.

In the case of a significant increase in stress, failure may occur, and since the increase in stress is also directly proportional to Young's modulus, this effect will likely be more pronounced in stiff rocks and concretes.

The coefficients of thermal expansion of rocks and concrete take similar values of about 10^{5} $°C^{-1}$, so assuming the values of Young's modulus of 30 GPa and the Poisson's ratio of 0.2, the increase in stress will be of the order of 0.375 MPa/°C.

Assuming that the temperature of rocks at a depth of 10 m is 10 °C, and the temperature of compressed air or water in the storage is 35 °C, and that the temperature gradient of rocks is equal to 0.03 °C/m, Young's modulus is 30 GPa, Poisson's ratio is 0.2 and the coefficient of thermal expansion of concrete is 1.2 10-5 $^{oC-1}$ the increase in stress at shallow depths (0 -50 m) will reach approx. 11 MPa. Thermal stress will have a favorable effect on the stability of the shaft lining at these shallowest depths, so that even at the maximum forecasted medium pressure of 8 MPa, the condition indicating the danger of fracturing will not be met.

At greater depths, where there is a risk of shear damage to the casing, especially with not the highest limit strength values for uniaxial compression of concrete, the temperature increase in the values of vertical and circumferential stresses contributes to the increase of the damage zone and requires attention.

There remains to consider the issue of large depths, at which the primary temperature of the rocks can exceed that of compressed air or water, in this case there will be cooling of the casing and rocks in its vicinity and the value of σ_z i σ_θ will decrease slightly. Due to the small temperature differences, this effect will be small, but beneficial and the risk of damage to the enclosure will be reduced.

4. Real case scenario example

For the purpose of analysis, an underground working surrounding one of the shafts in one of the coal mines at the Upper Silesia Coal Basin was considered. The working is located at the level 1000 m below ground level and the volume of horizontal working surrounding the shaft in the form of the ring with cross section channels was assumed as a lower reservoir. The shaft has a circular cross-section and is lined with reinforced concrete, widely used in underground mining infrastructure due to its durability and resistance to pressure.

The analysed case, located at a depth of 1000 m and connected to the surface by a shaft with a diameter of 9.5 m, assumed the use of specialized and chamber workings around the shaft with a total length of 1026 m shown on figure 8. Considering the dimensions of the support structure, namely a height of 6.25 m and a width of 5.25 m, with steel arch support, the total volume of the specialized and chamber workings in the analysed shaft bottom is 55,791 m³. Additionally, the total volume of the shaft itself available for water storage (roughly 50 m) is 4,625 m³.
However, it is worth noting that this example refers to the design dimensions of the support structure. Unfortunately, in the studied case, significant convergence (Figure 7, Tabele 2) of the support occurred during the mining operation.
Convergence of the mining support refers to the phenomenon of the walls of a mining excavation moving closer together as a result of rock mass stresses. This occurs primarily in underground conditions, where the extraction of a deposit leads to changes in the stress equilibrium in the vicinity of the excavation.
The cause of convergence is the deformation of the rock mass under the influence of forces acting towards the excavation, leading to a gradual reduction of its cross-section. This phenomenon can be particularly intense in rock masses with low strength, significant fracturing, or under conditions of high geostatic stress.

Convergence can negatively impact the stability of the excavation, making it crucial to monitor the displacements of the support structure and use appropriate reinforcements, such as rock bolts, steel meshes, or shotcrete. In extreme cases, convergence can lead to collapses or the destruction of the excavation, posing a threat to worker safety and the continuity of mining operations.

As it was discussed in Deliverable 2.2 the workings should have a full concrete support with a circular cross-section that will prevent from convergence. Additionally, by using excavations that have been subject to convergence for several decades, we will face a challenge of using an excavation that may be almost half the size of the originally designed excavation (Fig. 6). Taking the above into consideration, the available area of special and chamber workings will be reduced to 8500 m³ in case under research.

Fig. 6. Graphic representation of the convergence of the working and proposed lining method for the purpose of construction of underground water reservoir ducts

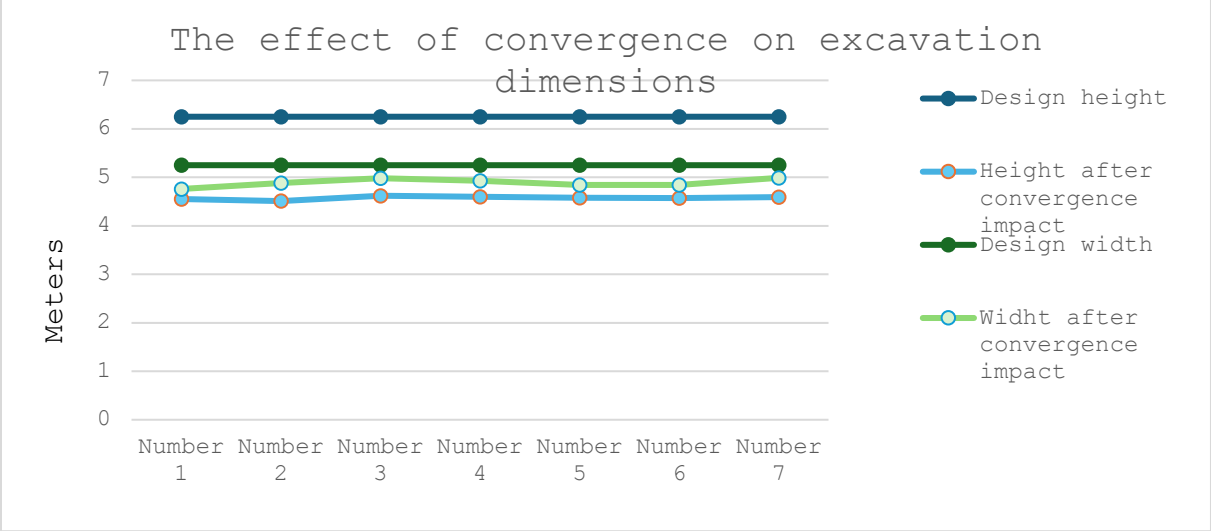

Fig. 7. Convergence of underground workings measured in the mine

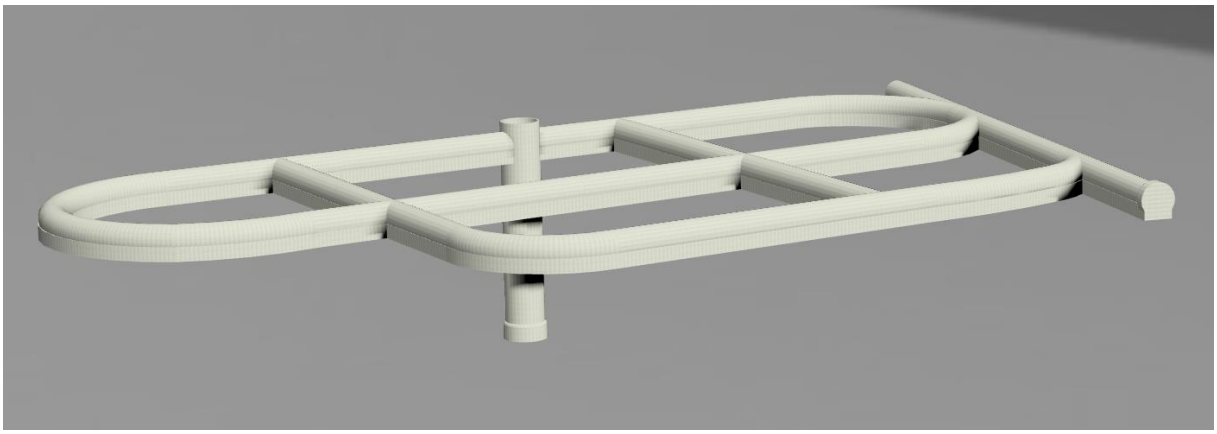

Fig 8. Geometry of special forking surrounding shaft

The lining has a thickness of 45 cm, providing robust structural support. The material properties of the lining, such as compressive and tensile strength, ensure its performance under varying working conditions, including cyclic changes in internal pressure ranging from 2 MPa to 8 MPa. The surrounding rock mass consists of layered clay shale, which features block structures with distinct fracture orientations and spacing, typical for deep mining environments.

The shaft and its surrounding rock mass are subjected to anisotropic stress conditions, with vertical stress values reaching 25 MPa, horizontal stress in one direction of 25 MPa, and a lower horizontal stress of 12.5 MPa in the orthogonal direction. These conditions reflect the influence of overburden weight and geological features at the analyzed depth.

This configuration, combined with the thermal conditions within the shaft, such as a temperature gradient of 0.03°C/m and internal medium temperatures ranging between 30–40°C, ensures that the shaft can be evaluated for its suitability as a compressed air energy storage (CAES) system or as part of a pumped-storage hydroelectric plant infrastructure.

Table 2. Dimensional parameters

Parameter	Value	Value after convergation
Shaft diameter	9,5m	
Workings width	5,25m	4,75
Workings height	6,25	4,50

4.1. Numerical modeling

The study focuses on the stability of the shaft lining under cyclic pressure loads and examines the interaction between the reinforced concrete lining and the fractured rock mass, assessing deformation, stress distribution, and potential failure mechanisms. The parameters for the study are presented in tables 3,4,5,6.

Table 3. Shaft Lining Parameters

Parameter	Value
Young's Modulus (E)	30 GPa
Young's Modulus (E)	30 GPa
Poisson's Ratio (ν)	0.2
Lining Thickness	45 cm
Lining Material	Reinforced Concrete
Internal Friction Angle (φ)	41°
Dilatancy Angle (ψ)	2.05°
Compressive Strength (Rc)	24–45 MPa

Table 4. Rock Mass Parameters

Parameter	Value
Rock Type	*Clay Shale*
Young's Modulus (E)	*5700 MPa*
Poisson's Ratio (v)	*0.24*
Compressive Strength (σC)	*47.6 MPa*
Tensile Strength (σT)	*0.89 MPa*
Cohesion (c)	*3.7 MPa*
Internal Friction Angle (φ)	*33°*
Rock Structure	*Layered-Block*
Fracture Orientation	*70° and 150°*
Fracture Spacing	*25–30 m*

Table 5. Pressure and Temperature Parameters

Parameter	Value
Working Pressure	2–8 MPa
Maximum Lining Displacement	10.1 mm
Range of Hoop Stress	60–65 MPa
Medium Temperature	30–40°C
Rock Temperature Gradient	0.03°C/m
Thermal Stress	0.375 MPa/°C

Table 6. Stress parameters

Parameter	Value
Vertical Stress (σz)	25 MPa
Horizontal Stress (σx)	25 MPa
Horizontal Stress (σy)	12.5 MPa
Fracture Pressure	~8 MPa
Maximum Fracture Risk Depth	80 m
Lining Stability	Shear and Fracture Failure Analysis

4.1.1. Analysis goal

The aim of the analysis was to investigate how the process of water pumping to the pressure of 8 MPa (and then its cyclic expansion and compression) or analogous changes in water pressure in the shaft will affect the state of stress, deformation and strain of both the shaft excavation lining and the rock mass in its vicinity.

4.1.2. Model description

A numerical model of a layered-block, fractured rock mass was constructed, and a numerical simulation was carried out under conditions of a highly anisotropic stress state affecting the lining of underground workings (shafts or tunnels). The task was performed using the UDEC code based on the Distinct Element Method, which is dedicated to geomechanical analyses of discontinuous and anisotropic media, such as rock masses where mining excavations are typically developed (see Itasca, 2011).

4.1.3. Structural model of the rock mass

A numerical model of a layered-block, fractured rock mass was constructed, and a numerical simulation was carried out under conditions of a strongly anisotropic stress state acting on the excavation linings (shaft or drift). The task was performed using the UDEC code based on the Distinct Element Method, which is dedicated to geomechanical analyses in discontinuous, anisotropic media, such as rock masses, where mining excavations are typically made (see Itasca, 2011).

The model is a rectangular plate with unit thickness, placed in a plane strain condition. It has a length of 75 m and a height of 50 m. In the central part of the model, the presence of two excavations was simulated, understood either as vertical shafts or as horizontal drift excavations with a circular cross-section: a larger one with a diameter of 9.5 m (at the opening) and a smaller one with a diameter of 5.24 m (we assume maximum available space in the working that could be available with minimum support) that more accurately reflect the geomechanical conditions

in which mining excavations are made in rock masses, the assumption of homogeneity and isotropy of the rock medium in which these excavations are located was abandoned. The model plate was divided into blocks by introducing horizontal planes with limited cohesion, and then smaller blocks were generated within them (see Figure 9).

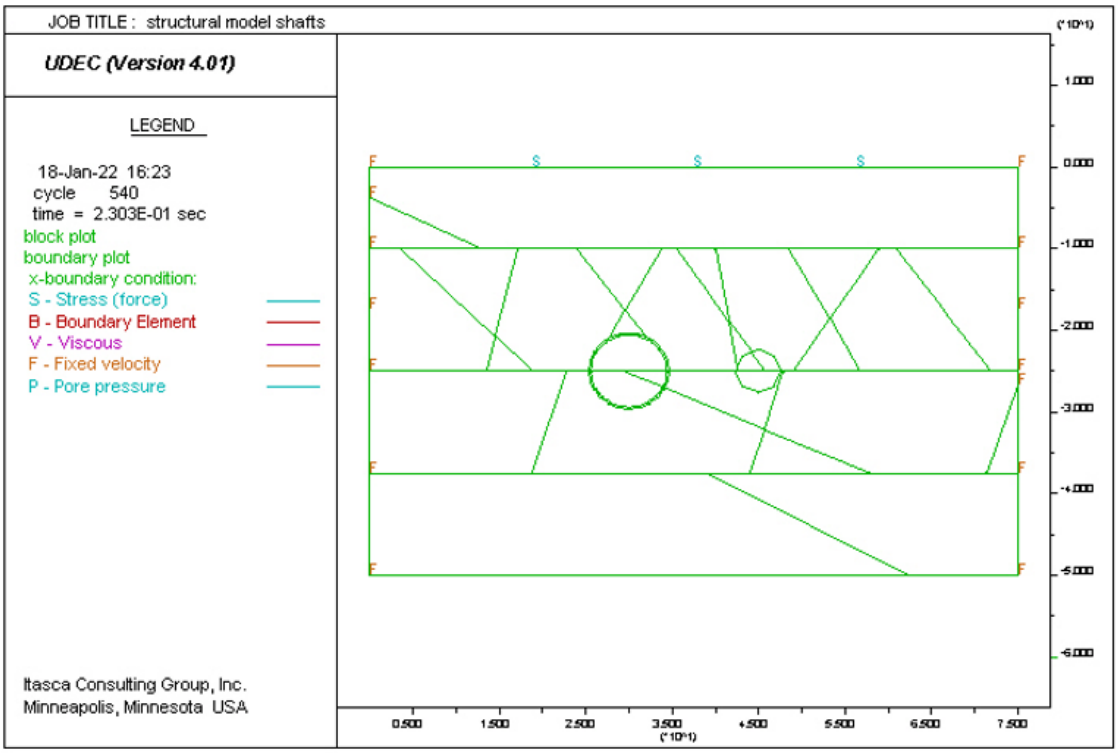

Fig. 9. Structural model of the rock mass surrounding the excavations and boundary conditions.

Individual horizontal areas have been divided into blocks by a system of weakening planes. In those furthest from the workings, the existence of a single system of cracks oriented at an angle was assumed α equal to approximately 70° and the average distance between the cracks equal to 30 m, and in these middle two systems of cracks with medium angles α_1 ~70° i α_2 ~ 150° i 25 m the average distance between cracks. By entrusting the computer with the automatic generation of weakening planes (contacts between blocks), only the average value of angles α and standard deviation was determined. These systems of planes of reduced cohesion divided the rock mass model into 38 blocks of average size equal to 122,3 m^2 (min. 0,42 m^2, max. 669,1 m^2) 189 contacts (Fig. 2). The number of zones (triangular finite difference elements) into which the blocks were divided, and the number of mesh nodes were equal to 215 and 263, respectively.

4.1.4. Physical model of a rock massiff

The rock blocks were assigned an elastoplastic material model with the strength limit described by a modified Coulomb failure criterion. The following material constants are associated with this model: bulk modulus (K), shear modulus (G), internal friction angle (ϕ), cohesion (c), tensile strength (σT), and dilatancy angle (ψ). It was assumed that the material of the rock blocks is clay shale, and the values of the material constants characterizing this unaltered rock material are provided in Table 7.

Tabel 7. Values of mechanical parameters of rock material building rock blocks in a rock mass model with a layer-block structure.

rock	ρ	E_M	ν	σ_C	σ_{CM}	ϕ	$N\phi$	c_M	σ_{TM}	ψ	G	K
	kg/m^3	MPa		MPa	MPa	deg		MPa	MPa	deg	MPa	MPa
Clay shale	2650	5700	0,24	47,6	13,6	33	3,4	3,7	0,89	16,5	2298	3654

ρ – bulk density,
E_M – Young's modulus (in the rock mass),
ν – Poisson's ratio,
σ_C – uniaxial compressive strength of the rock material,
σ_{CM} – uniaxial compressive strength (in the rock mass),
ϕ – internal friction angle,
N_ϕ – coefficient appearing, among others, in the strength criterion of Coulomb expressed in terms of stresses. main, $N_\phi = \frac{1+\sin\phi}{1-\sin\phi}$, c_M – cohesion (in the massif), σ_{TM} – Ultimate tensile strength (in solid), □ - dilation angle.

The contacts between the blocks were assigned a mechanical model capable of normal and shear elastic deformations, as well as plastic, dilatational slip with weakening, and tensile separation. When modeling the behavior of the contacts between the blocks, it was assumed that the relationship between the increments of the effective normal stress (Δσn) and the corresponding displacement increments in the direction perpendicular to the contact plane is linear, given by the equation:

$$\Delta\sigma_n = k_n \Delta u_n \qquad (30)$$

where k_n is the coefficient of the normal stiffness of the contact. Equation (30) is valid for both compressive and tensile stresses if only $\sigma_n \geq -\sigma_{Tj}$, where σ_{Tj} s the tensile strength limit of the contact. If this limit is exceeded ($\sigma_n < -\sigma_{Tj}$), then the contact stops transmitting normal stresses, a so $\sigma_n = 0$.

It was assumed that the relationship between the increments of shear stress (Δτs) and the increments of the elastic shear displacement component is also given by a linear equation of the type (30). (Δu_s^e):

$$\Delta\tau_s = k_s \Delta u_s^e \qquad (31)$$

The proportionality coefficient in this equation is the so-called contact shear stiffness coefficient (ks). Equation (31) applies to shear stresses that satisfy the Coulomb failure criterion.

$$|\tau_s| \leq c_j + \sigma_n \operatorname{tg}\phi_j = \tau_{ult} \qquad (32)$$

where c_j denotes cohesion, a ϕ_j - is the friction angle on the contact surfaces. In the stage after the shear strength limit of the contact is exceeded, meaning when $|\tau_s| > \tau_{ult}$, the condition $\tau_s = \text{sign}(\Delta u_s)\ \tau_{ult}$, where Δu_s is the increment of the total shear displacement. In this stage, the cohesion values (c_j) are reduced to zero.

It was also assumed that the exceeding of the shear strength limit of the contact and the occurrence of inelastic slip between the rock blocks is accompanied by the dilation effect, i.e., the opening of the contact surfaces, which depends on the magnitude of the dilation angle. ψ_j. Dilation is a function of the shear direction: it increases or decreases depending on whether the

sign (direction) of the shear displacement increment is in the same or opposite direction to the sign of the total shear displacement.
The dilatational component of the normal displacement (u_n^d) decreases with the increase of normal stress. (σ_n) the dilation effect completely disappears ($\psi_j = 0$), when the shear displacement exceeds a certain critical value. u_{cs}. This limitation of dilation in the basic model for the UDEC program, though not the only one, is related to the actual degradation of roughness on the fracture walls in rocks. Crushing and smoothing of the roughness progress as the shear path increases; this effect is favored by high normal forces.
The values of the material constants relevant to the contact model used for the calculations — the normal stiffness coefficient (kn), shear stiffness coefficient (ks), friction angle (ϕj), cohesion (cj), tensile strength limit (σTj), and dilation angle (ψj) — are listed in Table 8.

Table 8. Material constants for the contact models between rock blocks used in the calculations.

Layer	k_n	k_s	φ_j	c_j	σ_{Tj}	ψ_j
	[MPa/m]	[MPa/m]	[deg]	[MPa]	[MPa]	[deg]
Clay shale	5500	2200	16,5	0,185	0,015	1,65
Reinforced concrete lining	9550	4011	41,0	26,000	6,500	2,05

4.1.5. Boundary and initial conditions

In the rock mass model, mixed displacement-stress boundary conditions were set. It was assumed that the nodal points on the vertical, side edges of the model are free to move in the vertical direction, while their horizontal displacements are set to zero. Nodes located on the bottom edge of the model can move horizontally, while their vertical displacements are set to zero. The remaining nodal points were allowed to move freely in any direction. A primary stress was applied to the upper edge of the model (see Figure 6).
When setting the initial stress state in the model, it was assumed that the vertical stress in the rock mass is due to the gravitational forces and is determined by the bulk density of the rocks, soil, and coal. Furthermore, to examine the effect of the highly unfavourable stress state that may exist in excavated shaft or drift tunnels with a circular cross-section, it was assumed that the stresses in one of the horizontal directions (x) would be approximately equal to the vertical stress, while the stresses in the orthogonal direction (y) would be about half of the stresses in the x and z directions.
It was assumed that the vertical component of the initial stress state and the horizontal component in the x direction $(\sigma_{ZO} = \sigma_{XO})$ are equal to approximately 25 MPa, and the horizontal component in the direction of y (σ_{YO}) is about 12.5 MPa. The above assumption, assuming that the vertical stress comes from the weight of the overlying rocks, means that the model plate is located at a depth of about 1000 m.
The calculations were then started; In the course of reaching the initial equilibrium state in the model, the original state of stress was established. Only then did I start the simulation of the excavation of the workings, the construction of a tight reinforced concrete support and the proper analysis of the influence of the variable pressure of the medium in the shaft (resulting from the cycles of compression and expansion of air inside the shaft as an energy storage or

variable in height of the water column in the shaft which is an element of the pumped-storage power plant).

4.1.6. Model of shaft pit support as energy storage

The lining of the shaft excavation intended as an energy storage facility was modelled as a ring filling the shaft/working along its entire perimeter. It was assumed that the thickness of the ring would be 45 cm, and its properties correspond to those of reinforced, watertight concrete commonly used in underground construction, including in shafts. It was also assumed that its behavior, like the rock material of the surrounding rock mass, follows Hooke's law until the failure limit is reached, and the failure limit in a combined stress state is defined using the Coulomb (Coulomb-Mohr) failure criterion. The material constants characterizing the energy storage lining used in the numerical model, as well as those defining the contact properties between the lining concrete and the surrounding rocks, are provided in Tables 2 and 3, respectively.

4.1.7. Numerical simulation of shaft drilling in a block-layer rock mass and analysis of its condition before the construction of an energy storage facility inside

Before starting the simulation of the shaft operation as an energy storage, we performed a simulation of the excavation of the workings and bringing the model to a state of equilibrium, which was aimed at mapping the long period of existence of the mining workings and determining the state of stress, displacement, deformation and effort.

To understand the behavior of the excavation lining and the surrounding rock mass during the increase of the medium pressure to a high level of around 8 MPa (and its subsequent cyclic reduction and increase), several locations for detailed monitoring of changes in stress, strain, and displacement were selected in the numerical rock mass model.
For a more accurate investigation of the deformation process of the lining, monitoring points for displacement (Figure 9) and stress and strain (Figure 10) were located at four points of the lining: the northern, southern, eastern, and northwestern parts.

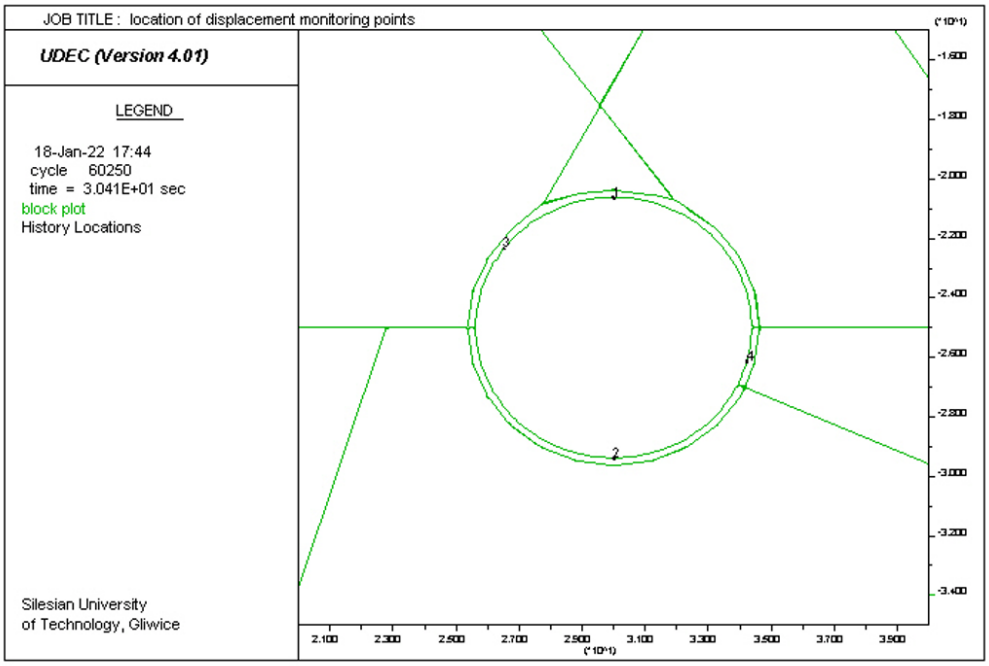

Fig. 10. Locations for monitoring the displacement of casing points during the simulation of air compression and expansion cycles inside the shaft.

During the excavation, the shear strength limit was exceeded in the rock block located near the northern part of its lining and in one area near its western side (Figure 11). The shear strength limit was also reached in a small section of the lining itself (on the eastern side). In the simulation of the cycles of increasing and decreasing the medium pressure inside the excavation, it was also examined whether local damage to the lining, assuming its integrity, would propagate during periodic pressure changes and the operational phases of the energy storage system.

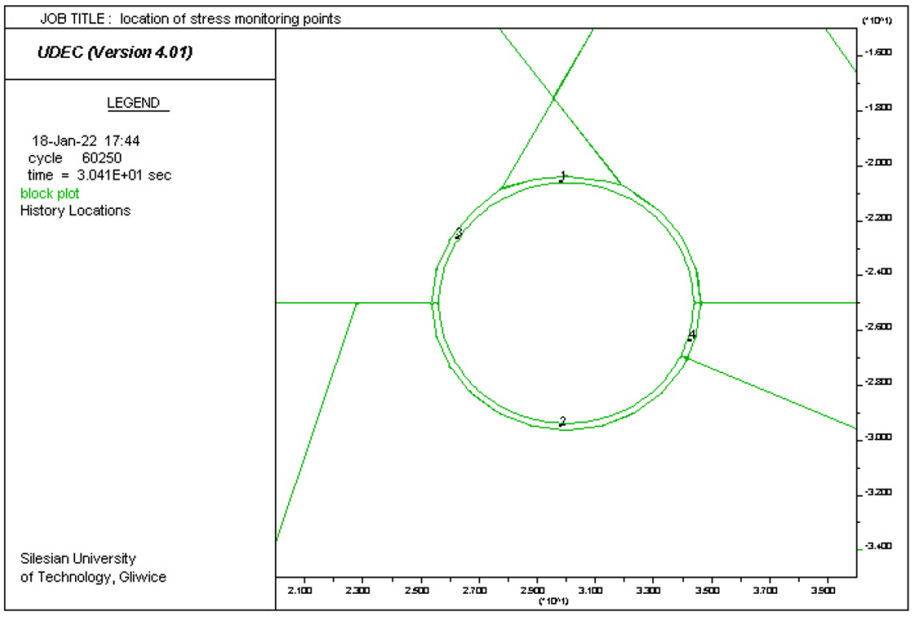

Fig. 11. Stress monitoring locations in the enclosure.

The process of increasing the medium pressure in the excavation was simulated by gradually increasing the pressure applied to the inner side of the lining by 0.1 MPa and bringing the model to equilibrium. This approach allows for reproducing the expected course of the real pressure increase process and avoids the sudden loading of the excavation lining and the surrounding rocks.

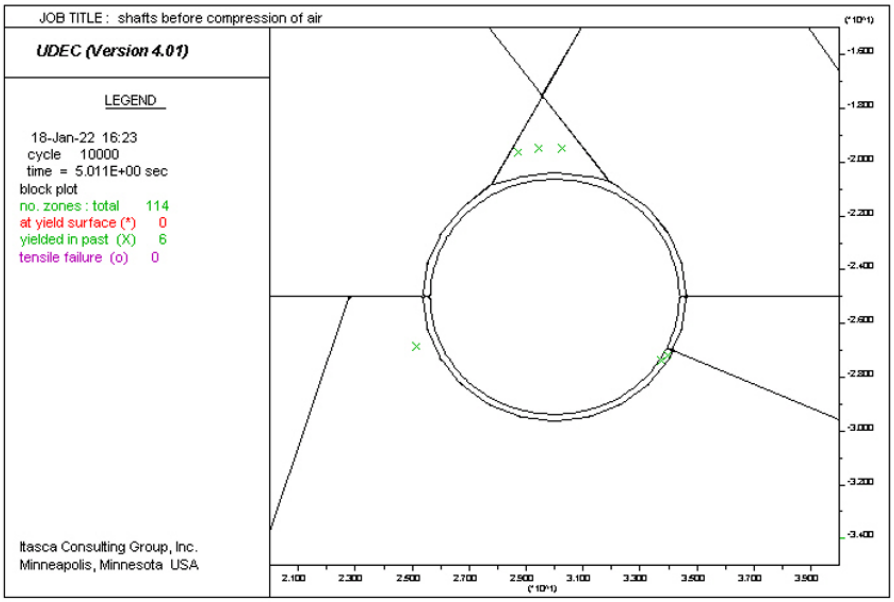

Fig. 12. Areas in the rock mass model and in the roadway support where the shear limit strength has been reached before the first cycle of increasing the pressure of the medium.

The first pressurization cycle was carried out from atmospheric pressure in 80 steps to 8 MPa (80 bar). The first cycle of reducing the pressure of the medium in the excavation was simulated analogously in 60 steps, reducing the pressure by 0.1 MPa to 2 MPa, and then again in stages, increasing the pressure to 8 MPa, simulating the second cycle, e.g. air compression.

4.1.8. Simulation of pressure increasing and decreasing cycles in the excavation

The most important stage of the analysis was to examine the impact of the cycles of increasing and decreasing the pressure of compressed air or water on the state of the excavation lining and the surrounding rock mass. The main excavation will serve as the energy storage, while the excavation with a smaller diameter in its vicinity will serve a supporting, service function.

Increasing the pressure to 8 MPa in the first cycle, gradually reducing it to 2 MPa in the first unloading cycle, and the subsequent pressure increase cycle do not cause any cracking of the lining or the surrounding rock material, whether due to shear or tensile stresses (Figure 10).
The process of increasing the pressure induces deformation of the lining and the adjacent rock. Since the excavation was made not in a homogeneous, continuous, isotropic rock mass, but in the presence of planes of limited cohesion and rock blocks of varying sizes, the displacement of the excavation contour is not uniform. At the maximum pressure value applied, the extreme displacement value is about 10.1 cm and occurs in the northern part of the excavation lining.
The numerical marker in the northern part of the excavation lining (marked as #1 in Figure 7) moves in the positive Y-axis direction by a maximum of 10.1 mm during the first pressure increase cycle. Reducing the compressed air or water pressure causes it to move toward the

center of the excavation, with the displacement reaching about 2.5 mm from the initial position at the lowest pressure value (2 MPa) (Figure 11).

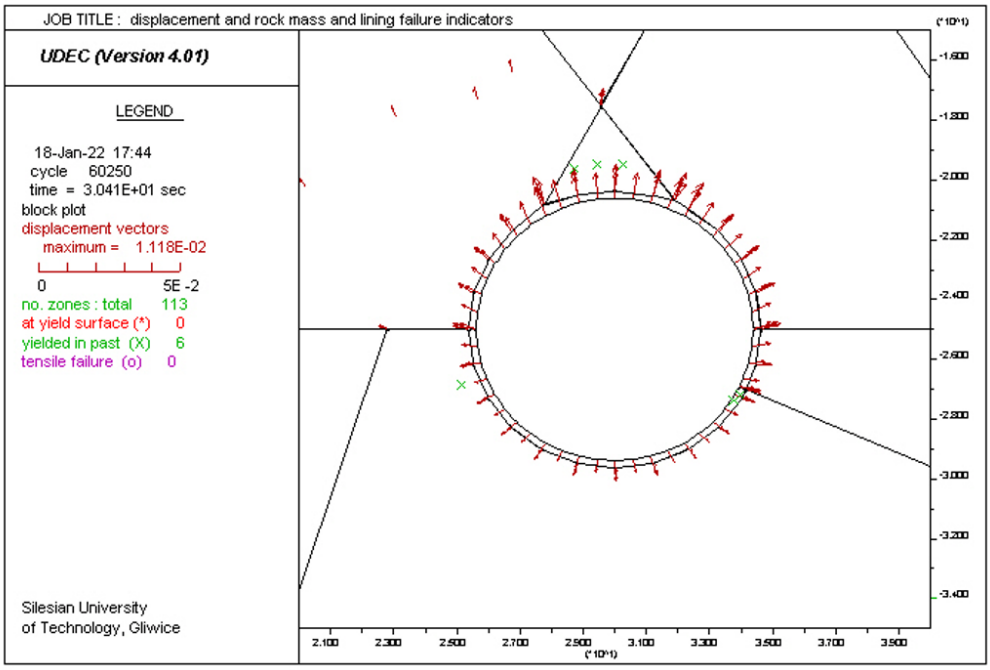

Fig. 13. Displacement vectors and places where the shear limit strength was reached at the end of the second pressurization cycle.

The movement of the point located in the southern part of the lining (number 2 in Figure 11) follows a similar pattern, but the maximum displacement values are noticeably about half as large. The maximum displacement in the southern direction reaches just under 5 mm (4.89 mm), and its position at the minimum medium pressure in the energy storage system remains about 1.5 mm further from the center of the excavation than it was before the first pressure increase cycle. The main cause of the difference in displacement values between the northern and southern parts of the lining seems to be the presence of fractures and the rock block formed by them directly to the north of the excavation lining, in direct contact with it.

The displacement in the Y direction of the point located in the northwestern part of the lining, which is represented by the red polyline in Figure 11, is noticeably smaller than that of the point located in the exact northern part of the lining. This is obviously due to the fact that the radial movement of this point, in addition to a high displacement component in the Y direction, also has a similar displacement in the X direction (see Figure 13, cyan-colored line). The displacement in the Y direction of the point in the eastern part of the lining is very small (max. about 0.3 mm), and its movement mainly occurs along the X axis, with the maximum displacement to the east from the center of the excavation at a pressure of 8 MPa reaching just under 6 mm. Similarly, the displacements in the X direction of the points in the northern and southern parts of the lining are very small, on the order of tenths of a millimeter at most (Figure 13).

The extreme displacement values of several millimeters mean that the relative elongation of the excavation cross-section does not exceed 0.2% in either the X or Y direction.

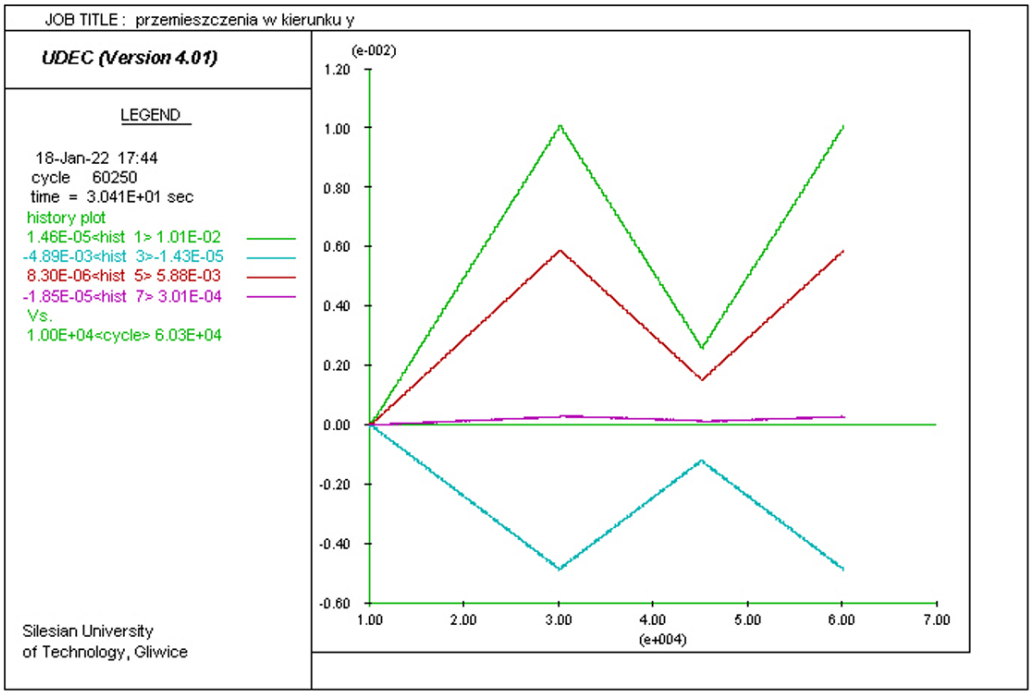

Fig.14. Graph of the values of displacements in the y-direction for selected monitoring locations.

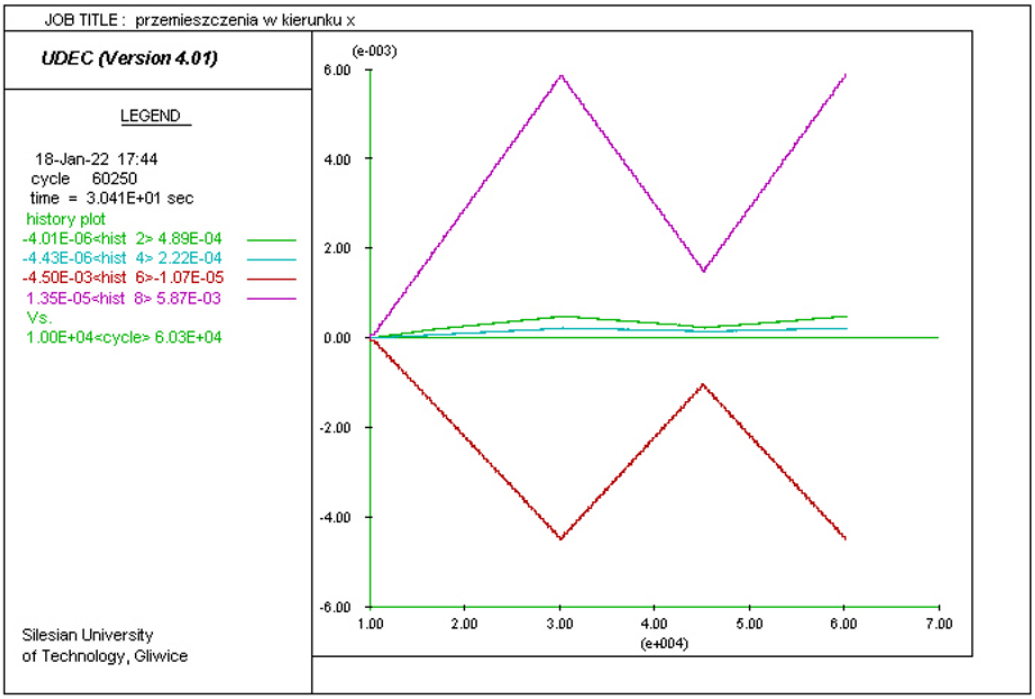

Fig. 15. Graph of the value of displacements in the x-direction for selected monitoring sites.

The process of pressure reduction induces elastic deformation of the lining, with the points moving toward the interior of the excavation. However, they do not return to their initial position due to the assumed minimum pressure in the energy storage system of 2 MPa (compared to 0.1 MPa initially). The subsequent pressure increase (second cycle) results in the same displacement of the lining points as was recorded during the first loading (compression) cycle.

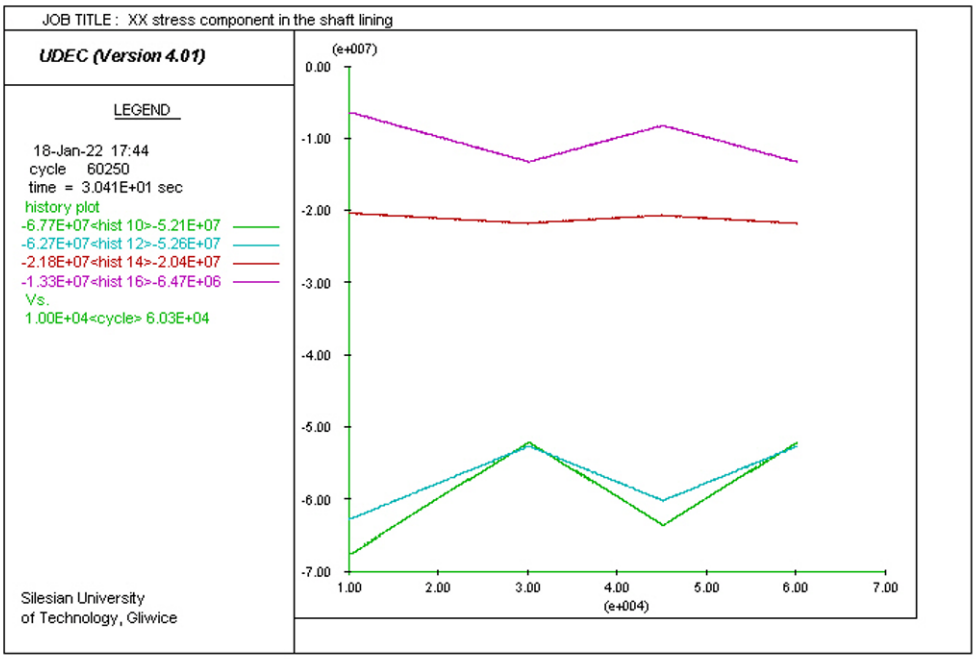

Fig.16. Changes in the value of the normal component of stress in the X direction (σξ) at selected monitoring sites.

Monitoring the components of the stress tensor allows for observing changes in the stress state of the lining during the cycles of increasing and decreasing the medium pressure in the excavation. The plots of the normal stress component in the X direction at points 1 and 2 (numerical markers for the northern and southern parts) shown in Figure 13 are particularly interesting. The normal component in the X direction can be approximately identified with the circumferential stress at these points. According to the Kirsch solution, the value of the circumferential stress, with the assumed initial stresses of approximately 25 MPa (σx) and 12.5 MPa (σy) as used in the simulation, is around sixty MPa at these points. Such values are also observed in the numerical model (cyan and green curves in Figure 13). The process of increasing the pressure causes a decrease in the value of this stress in the lining, and reducing the pressure leads to an increase. However, even at the minimum pressure of the medium in the excavation (2 MPa), the high circumferential stress values undergo noticeable reduction.

5. Summary

The search for possibilities for the economic use of post-mining excavations, especially shafts, has been ongoing in Poland and worldwide for some time. The intensification of this work has occurred in recent years due to the so-called green transition. One of the more promising directions seems to be the use of the shaft as an energy storage system, such as Compressed Air Energy Storage (CAES), or as part of the infrastructure of a pumped-storage hydroelectric power plant. This project is another step toward exploring the potential use of decommissioned mining excavations in this role.

Within the scope of this project, stability analyses of a vertical shaft and horizontal workings subjected to the action of medium pressure (compressed air or water) and variable temperature inside it were performed under conditions of an isotropic stress state in the rock mass using an

analytical approach. For this purpose, the Coulomb (Coulomb-Mohr) failure criterion was used, along with the advances in rock mechanics for applications in petroleum engineering. A detailed analysis was conducted to determine the conditions required for shear failure or fracturing to occur at the excavation boundary of the shaft subjected to the action of working medium pressure inside it, in a field of compressive stresses or tensile failure upon reaching the tensile strength limit.

The method used for these analyses represents a departure from the post-war methodology of shaft stability analysis, which was developed in Poland until the 1990s and based on the use of soil mechanics principles. The equations and methods for describing the behavior of granular and/or low-strength and cohesive materials were abandoned. The vast majority of deep shafts cut through rock layers of significant strength, not soil-like media.

The widespread use of equations and solutions applicable to granular media in shaft lining design has often led to their over-dimensioning (see, e.g., Kwaśniewski, 1973; 1975). Currently, this is beneficial in the potential adaptation of shafts as energy storage systems, as the existing shaft linings, despite aging and concrete degradation, will not require as significant reinforcement as linings with smaller thickness.
As a result of the analytical work, a complete solution was developed, which allows estimating both the safe pressure ranges for compressed air or water inside the shaft and the depth ranges where there may be a need for reinforcement of the lining due to the risk of cracking, either from shear or tensile failure.

An important outcome of this project is the development of a dedicated application written in Python. This application is based on the geomechanical model and analytical methods presented in this report. It provides a practical tool for calculating the geomechanical stability of shafts and horizontal workings under varying conditions of stress, pressure, and temperature. The application automates complex calculations, allowing users to input specific parameters and obtain results related to shear or tensile failure risks, required reinforcement zones, and thermal stress impacts. A screenshot of the application interface and an example of its output can be found in Figure 16 & 17. This tool not only validates the methodologies developed in this work but also offers a practical way to apply them in future projects aimed at adapting mining excavations for energy storage purposes.

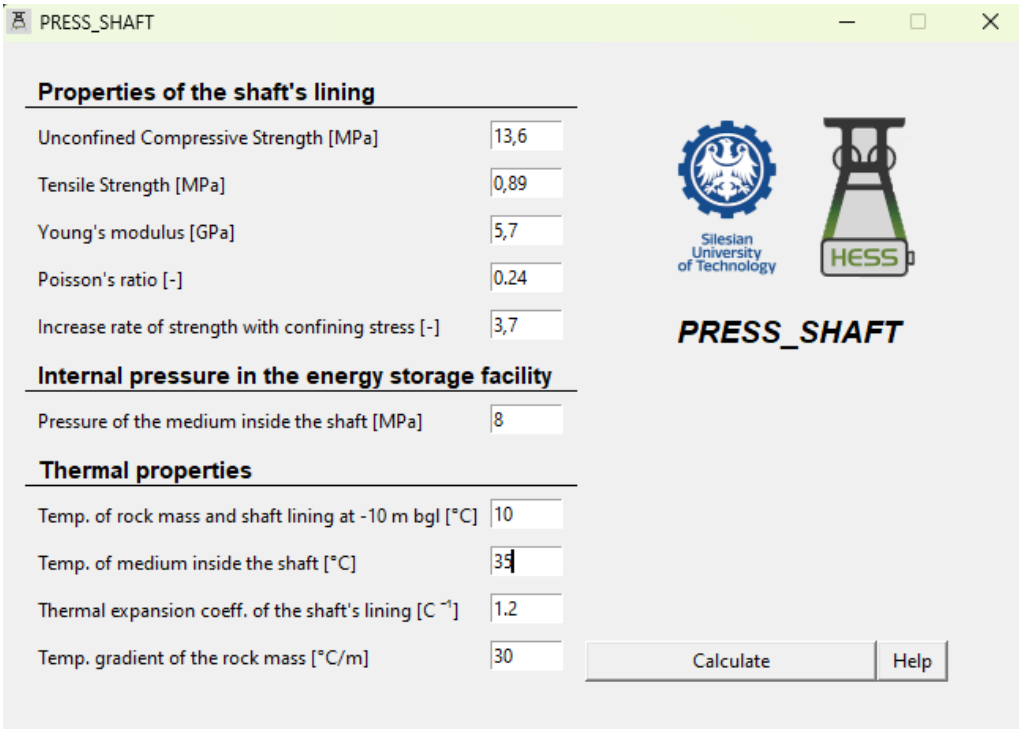

Figure 16. Interface of app with data from real case scenario.

PRESS_SHAFT

h [m]	Shear failure	Tensile failure	Zero tensile strength
10.0	stable	hydraulic fracture	hydraulic aperture
20.0	stable	hydraulic fracture	hydraulic aperture
30.0	stable	hydraulic fracture	hydraulic aperture
40.0	stable	hydraulic fracture	hydraulic aperture
50.0	stable	hydraulic fracture	hydraulic aperture
60.0	stable	hydraulic fracture	hydraulic aperture
70.0	stable	hydraulic fracture	hydraulic aperture
80.0	stable	hydraulic fracture	hydraulic aperture
90.0	stable	hydraulic fracture	hydraulic aperture
100.0	stable	hydraulic fracture	hydraulic aperture
110.0	stable	stable	hydraulic aperture
120.0	stable	stable	hydraulic aperture
130.0	stable	stable	stable
140.0	stable	stable	stable
150.0	stable	stable	stable
160.0	stable	stable	stable

Figure 17. Application results for the case in question

This project also analysed the impact of temperature on the stability of the shaft excavation. The thermal stresses that may occur in the shaft lining and the surrounding rocks at various depths were estimated, and the rock and rock mass properties as well as the concrete lining that these stresses depend on were provided. This part of the analysis allows for the preliminary identification of locations (depths) where there may be a potential risk of shaft lining damage due to thermal stresses.

The analyses performed in this work were based on the assumption that the shaft lining and the rock layers in the immediate vicinity of the shaft are drained, and that consequently, only negligible pore pressures occur. In situations where significant pore pressures might occur, the method for considering them in the stability analysis was provided.

The analytical work was carried out for an isotropic stress state, meaning that the horizontal stresses acting on the shaft lining are equal in magnitude. This state, although optimal from a geomechanical point of view and highly likely for many locations, is certainly not the only one in which an energy storage system could be built. The analysis of the impact of anisotropic stress states on the stability of a shaft or a circular cross-section drift excavation subjected to the processes of increasing and decreasing the working medium pressure inside it was carried out based on numerical modeling and computer simulations.
The tool used – the UDEC code for the Distinct Element Method – allows for the abandonment of the assumption of homogeneity and continuity of the rock mass and enables the simulation of conditions that could potentially occur at a selected depth of 1000 m in a typical shaft or drift excavation in one of the Upper Silesian mines.

The numerical simulations, including cycles of increasing the working medium pressure inside the shaft to a significant pressure of 8 MPa, then reducing it to 2 MPa and increasing it again to the same pressure, allowed for the determination of the stress, strain, displacement, and stress states of both the shaft lining and the surrounding rocks.

It was found that the additional load on the lining due to the increasing pressure of the medium inside the excavation does not cause cracking of the lining, and that the lining and surrounding rocks deform elastically during the cycles of increasing and decreasing pressure. The deformation of the lining associated with the displacement of the shaft contour into the rock mass remains small, not exceeding 0.2%; the maximum displacement of the lining point (located in its northern part) reaches about 10 mm at the highest working medium pressure of 8 MPa.
The next steps in research could be further developments both in analytical work and numerical modelling.
In the first, analytical work made use of the commonly used linear Coulomb-Mohr failure criterion. Despite the passage of years since its formulation (at the turn of the 18th and 19th centuries), it remains the most popular of the strength criteria used in rock mechanics, rock mass mechanics, and rock engineering. However, its application to the stability analysis of boreholes in various countries often leads to highly conservative results. Fracturing at the walls of boreholes does not occur as frequently as this criterion predicts (see, e.g., Fjær et al., 1992). Therefore, in recent years, there have been increasing attempts to replace it with one of the criteria that also considers the influence of intermediate principal stress on rock strength. Among these, the linear version of the Mohr criterion, the so-called Coulomb-Mohr criterion

(see, e.g., Al-Ajmi A.M. and Zimmerman R.W., 2006; Kwaśniewski, 2012), seems to be the most suitable and widely used.
In the second, since numerical modelling and computer simulations of cycles of increasing and decreasing working medium pressure inside the excavation, although advanced, used only one structural model of the rock mass and specific, though anisotropic, values of the initial stresses, the expansion and extension of such analyses with the construction of structural models with different, especially random, block divisions in different sedimentary rocks (not only clay shale, as in this case) or in different initial stress states seems necessary before any implementation of the concept of using a shaft or drift excavation as an energy storage system, whether for compressed air or as part of a pumped-storage hydroelectric power plant infrastructure.

6. Literature

7. Al-Ajmi A.M. and Zimmerman R.W. : *Stability analysis of vertical boreholes using the Mogi–Coulomb failure criterion.* International Journal of Rock Mechanics and Mining Sciences, Volume 43, Issue 8,pp. 1200-1211, 2006.

8. Biot M. A. : *Generalized theory of three dimensional consolidation.* Journal of Applied Physics, 12, pp. 155-164, 1941.

9. Biot M. A. : *Mechanics of deformation and acoustic propagation in porous media.* J. Appl. Phys. 33, pp. 1482-1498, 1962.

10. Fjær E., Holt R. M., Horsrud P., Raaen A. M. and Risnes R. : *Petroleum Related Rock Mechanics.* Elsevier Science Publishers, B.V. the Netherlands 1992.

11. Guenot A. : *Contraintes et ruptures autor des forages pétroliers.* In: Proceedings of the 6th International Conference on Rock Mechanics, pp. 109–118, 1987.

12. Habib P. & Berest P. : *Rock mechanics for underground nuclear waste disposal in France.* In: Comprehensive Rock Engineering. Vol. V, chapter 21, ed. J. A. Hudson, Pergamon Publication, Oxford 1993.

13. Hoek E. & Brown E.T.: *Underground Excavations in Rock.* Institution of Mining and Metallurgy, London 1980.

14. Jaeger J. C., Cook N. G. W. and Zimmerman R. W.: *Fundamentals of Rock Mechanics* (4^{th} edn). Blackwell Publishing, Malden 2007.

15. Kirsch E. G: *Die Theorie der Elastizität und die Bedürfnisse der Festigkeitslehre.* Zantralblatt Verlin Deutscher Ingenieure, Vol. 42, pp. 797-807, 1898.

16. Kwaśniewski M.: *Ciśnienie górotworu na obudowę szybu na dużej głębokości i jego wpływ na ustalenie rodzaju obudowy i sposobu jej obliczania*. Praca doktorska AGH, 1973.

17. Kwaśniewski M.: *Obliczanie betonowej obudowy szybowej w świetle rozważań teoretycznych oraz badań modelowych.* Zeszyty Naukowe AGH nr 476, Górnictwo z. 68, Kraków 1975.

18. Kwaśniewski M.: *Interpretacja fizykalna liniowego warunku wytrzymałościowego skał.* Wykład na XXIII Zimowej Szkole Mechaniki Górotworu, Bukowina Tatrzańska, marzec 2000.

19. Kwaśniewski M.: Recent advances in the studies of the strength of rocks under general triaxial compression conditions. Keynote address delivered by G. Smolnik at 41st Geomechanics Colloquium, Freiberg 2012.

20. Maury V. : *An overview of tunnels and boreholes failure mechanisms.* In: Comprehensive Rock Engineering, Vol. IV, chapter 14, ed. J. A. Hudson, Pergamon Publication, Oxford 1993.

21. Terzaghi K.: *Theoretical Soil Mechanics.* Wiley, New York 1943.

22. UDEC *User's Manual* (v. 5.0). Itasca Consulting Group, Inc., Minneapolis 2011.